Human balance control in 3D running based on virtual pivot point concept

Vahid Firouzi[1], **Fariba Bahrami**[1] **and Maziar A. Sharbafi**[2,*]

[1] Electrical and Computer Engineering Department, College of Engineering, University of Tehran, Tehran, Iran

[2] Lauflabor Laboratory, Technische Universität Darmstadt, Darmstadt, Germany

[*]Author for correspondence: sharbafi@sport.tu-darmstadt.de

Abstract

Balance control is one of the crucial challenges in bipedal locomotion. Humans need to maintain their trunk upright while the body behaves like an inverted pendulum which is inherently unstable. Instead, the virtual pivot point (VPP) concept introduced a new virtual pendulum model to the human balance control paradigm by analyzing the ground reaction forces (GRF) in the body coordinate frame. This paper presents novel VPP-based analyses of the postural stability of human running in a 3D space. We demonstrate the relation between the VPP position and the gait speed. The experimental results suggest different control strategies in frontal and sagittal planes. The ground reaction forces intersect below the center of mass in the sagittal plane and above the center of mass in the frontal plane. These VPP locations are found for the sagittal and frontal planes at all running speeds, respectively. We introduced a 3D VPP-based model which can replicate the kinematic and kinetic behavior of human running. The similarity between the experimental and simulation results indicates the ability of the VPP concept in predicting human balance control in running and can support its applicability for gait assistance.

[*]Author for correspondence: sharbafi@sport.tu-darmstadt.de

KEYWORDS: Balance control, Human running, template modeling, Virtual Pivot Point (VPP)

INTRODUCTION

Human leg morphology and motor control have evolved during thousands of years to perform various locomotion tasks over a wide repertoire of surfaces. Inspired by biological evolution, roboticists try to achieve similar capabilities in legged robots (Kim and Wensing, 2017). In that respect, simple template models like the spring loaded inverted pendulum (SLIP) (Blickhan, 1989) which can predict human leg function in the running were used to design and control legged robots (Ahmadi and Buehler, 1999; Hubicki et al., 2016). Further, quadruped robots such as MIT Cheetah can outperform humans concerning performance (speed) and efficiency (Seok et al., 2014). However, human capabilities in agile movement tasks such as running are still far beyond those of bipedal robots (Tajima et al., 2009).

Among different fundamental elements of legged locomotion, namely locomotor subfunctions (Sharbafi et al., 2017), upper body balancing is one of the most challenging ones. Bipeds are dynamically unstable and need to keep their trunk upright, especially inagile gaits like running. The increased complexity may result from the placement of more than 50% of total body mass in the upper body having significantly large inertia (Thorstensson et al., 1984). Because of that, small deviations in trunk position can significantly affect the whole body stability (Drama and Badri-Spröwitz, 2019). Nevertheless, humans benefit from the trunk's inertia to facilitate locomotion and can simply keep balance in running with minimal energy consumption (Bramble and Lieberman, 2004). Therefore, understanding balance control in running can simplify bipedal robot control (Sharbafi et al., 2016) and improve gait assistance with exoskeletons (Nasiri et al., 2018; Sugar et al., 2017).

Mechanics of balance can be understood in terms of how the ground reaction force (GRF) acting at the center of pressure (CoP) changes the body's angular momentum about its center of mass (CoM) (Popovic et al., 2005). Several methods were developed to quantify stability based on the relation between GRF, CoM, and CoP such as zero moment point (ZMP) (Kajita et al., 2007), foot rotation indicator (FRI) (Goswami, 1999) and centroidal moment pivot (CMP) (Popovic et al., 2005). In 2010, a new method was introduced by Maus et al., which could describe balancing in biological legged locomotion with a virtual pendulum (VP) model (Maus et al., 2010). They showed that the GRFs intersect near a virtual pivot point (VPP) above the center of mass (CoM) in the sagittal plane during human and animal walking (Maus et al., 2010). This method provides a template model for posture control, which does not need to measure body orientation with respect to the ground. Therefore, balancing can be achieved using the proprioceptive sensory signals, i.e., trunk to leg angle (Maus et al., 2010).

The VPP concept was not only utilized to predict biological gaits but also for the control of robots, e.g., ATRIAS robot walking (Peekema, 2015). Due to the bioinspired nature of the VPP concept, it has been also used to control assistive devices (Zhao et al., 2019; 2017; Firouzi et al., 2021). In the previous studies, generating a VPP above CoM was used as the control goal to achieve postural stability in different gaits in simulations and robots (Sharbafi et al., 2013; Maus et al., 2010). However, just a single study experimentally reported a VPP above CoM for running gait which is limited to only a single trial of a single subject without any statistical analysis (Blickhan et al., 2015). Recently, a simulation study using template models showed that intersecting GRFs below the CoM (resulting in negative VPP) could better explain running gait in the sagittal plane concerning the trunk angle (Drama and Badri-Spröwitz, 2019). Another study demonstrated similar negative VPP in human running at 5m/s (Drama et al., 2020).

Still, the VPP method was applied only to analyze running in the sagittal plane whereas lateral balance is even more critical in bipedal gaits (Kuo, 1999; MacKinnon and Winter, 1993). Humans prefer a narrow step width in running gait, which may make maintaining lateral balance more challenging (Arellano and Kram, 2011). From a broader perspective, although the majority of research on human gait has focused on the sagittal plane, movements in the frontal plane have particular importance for balance control (Krebs et al., 2002). In that respect, lateral stability in running gait needs further investigations.

In this study, we analyze human running in 3D, based on the VPP concept. We show that by choosing an appropriate coordinate frame, the VPP concept can also explain the relation between GRF, CoM and CoP in the frontal plane and consequently lateral balance control in human running experiments. Further, we explore the relation between VPP position and motion speeds. Then, we extend the template SLIP-based model of running with a trunk segment (called TSLIP) to employ the VPP to stabilize 3D running gait. The simulation and experimental results are compared which reveals potentials for future applications of this method to develop agile bipedal robots or assistive devices supporting human balancing in running gaits.

In the first part of this study, we analyze human running gait with the VPP landscape in the sagittal and the frontal plane. Our gait analysis involves humans running on a treadmill over a range of speeds. In the second part, we perform a simulation studyusing a template model to support our experimental findings in the 3D environment. Results of our simulation are compared with the human experiment to investigate the ability of our model to predict human kinematics and kinetics during running gait. Also, the robustness of our simulation is examined against perturbation in CoM velocity (representing an external push) when the position of the VPP is considered as a control target.

METHODS

This section describes the experimental data and explains how to verify the VPP in steady-state running gaits in the frontal and sagittal planes. Then, we present the method of applying VPP for control to generate stable running in a template-based 3D model.

Experimental data analyses

For studying VPP in human running, we borrowed the dataset from (Hamner and Delp, 2013), which is accessible at (dataset, 2013). The experiments include treadmill running of 10 male individuals (age: 29 ± 5 years, height: 177 ± 4 cm, mass: 70.9 ± 7 kg) at four running speeds. Each subject is an experienced long-distance runner who reported running at least $50 km$ per week. Positions of 54 reflective markers were measured at 100 Hz using eight Vicon MX40 + cameras. In addition to motion capture data, the ground reaction forces and moments were measured at 1000 Hz using a Bertec Corporation instrumented treadmill. Each subject ran between 15-20 steps at each speed. Marker positions and GRFs were filtered by a 15 Hz low pass filter with a zero-phase fourth-order Butterworth filter and a critically damped filter, respectively. The Stanford University Institutional Review Board approved the experimental protocol and subjects provided informed consent to participate. More details about the dataset can be found in (Hamner and Delp, 2013).

To analyze human balance control we utilized a 12-segment, 29-degree-of-freedom generic musculoskeletal model (Hamner et al., 2010) in OpenSim software (Delp et al., 2007). First, the model was scaled to match each subject's anthropometry based on experimentally measured markers placed on anatomical landmarks. Then joint angles were calculated using an *Inverse Kinematic Tool (IK)*. The output of the IK tool together with the GRF data were employed to compute the CoM and the virtual pivot point (VPP).

In an ideal VPP model, all GRF vectors starting from the CoP intersect in a single virtual pivot point in the body coordinate frame. In the experimental analyses, we define the VPP as a point that minimizes the time-integral of the difference between the original angular momentum and the angular momentum calculated if the GRF is passing through the VPP (see details in (Maus et al., 2010)). Based on this definition, Vielemeyer et al., introduced a measure called the coefficient of determination R^2 to evaluate the ability of the VPP model to predict human posture control (Vielemeyer et al., 2019). A comparable R^2 measure was used in (Herr and Popovic, 2008) to assess the amount of agreement between zero-moment model forces and measured horizontal forces in human walking. We adapt the R^2 measure proposed in (Vielemeyer et al., 2019) by considering the GRF magnitudes (normalized by the average GRF in stance phase) in the added weight W as follows:

$$R^2 = \left(1 - \frac{\sum_{i=1}^{N_t} \sum_{j=1}^{N_s} (\theta_{exp}^{ij} - \theta_{VPP}^{ij})^2 W^{ij}}{\sum_{i=1}^{N_t} \sum_{j=1}^{N_s} (\theta_{exp}^{ij} - \bar{\theta}_{exp})^2 W^{ij}} \right) \times \%100 \quad (1)$$

in which (θ_{exp}^{ij} and θ_{VPP}^{ij}) are the force vector angle taken at the j^{th} instant of gait cycle of the i^{th} trial for the experimental data and VPP model-predicted data, respectively. In the VPP model, the predicted force vector is from CoP to the VPP. The bar sign indicates the mean of the variables. N_t and N_s are the number of trails and the number of samples in each trial, respectively. In the ideal scenario, when all GRFs intersect at one focused point, $R^2 = 100\%$ is obtained, which means the VPP model can perfectly predict GRF's direction and human balancing as a result of the interaction with the ground, reflected in the GRF vectors. Low positive values for R^2 indicate that the estimation using VPP is almost similar to using the mean value $\bar{\theta}_{exp}$. In this study, we consider $R^2 = 70\%$ as a lower threshold to decide about VPP existence in a gait pattern.

In the following we describe VPP calculation in the sagittal and frontal planes:

VPP in the sagittal plane

The first step for finding the VPP is choosing an appropriate (reference) coordinate frame with respect to the human body. We define the reference frame in the sagittal plane with the origin at the body CoM while the upper-body direction (the hip to shoulder vector) determines the vertical axis (Maus et al., 2010) (Fig .1a). Also, we skip the data at the first25% of the stance phase to remove the impact effect. After transferring the GRF data from world frame to the defined reference frame, the VPP is calculated as instructed in (Maus et al., 2010).

VPP in the frontal plane

The reference frame in the frontal plane is also centered at body CoM, whereas the pelvis orientation defines the horizontal axis (Firouzi et al., 2019) (Fig. 1b). We tested several different orientations for the reference frame in the frontal plane (e.g., lumbar line) and the pelvis orientation provided the simplest and most accurate description of the GRF direction.

Previous studies (MacKinnon and Winter, 1993) also presented the significant contribution of pelvis to lateral balance control in the single support phase.

Simulation model

To predict humans balance control in running, we developed a 3D template model by extending the SLIP model with an additional trunk and damper. This model consists of a massless parallel spring-damper arrangement representing the virtual leg, beside a rigid trunk for the upper body with mass m and moment of inertia J, (see Fig .1c, d). Generating stable running with upright trunk (90°) using TSLIP (trunk+SLIP) is possible (Sharbafi and Seyfarth, 2014). However, to mimic human inclined upper-body posture with the template model, injected energy in the trunk should be dissipated. For this, we add a damper to the leg.

In our model, the virtual hip joint represents a point in the middle of the human left and right hip joints. The virtual leg is a segment that connects the virtual hip to the foot. The trunk orientation, defined by a line connecting the hip to the CoM, is characterized by the corresponding angles in the sagittal (ϕ_s), frontal (ϕ_f) and horizontal (ϕ_h) planes. By controlling hip torque in the sagittal and frontal planes in order to pass GRFs through VPP in these planes and choosing an appropriate leg adjustment strategy, stable human-like running can be achieved in 3D space.

The equations of motion are presented in Appendix A.

Control

The VPP model was already utilized to predict human-like hip torque and posture control in different gaits in the sagittal plane (Sharbafi et al., 2013;Maus et al., 2008). Here, we use this concept for posture control in 3D running using the template-based model described in "Simulation model" section and Fig. 1c, d. In the following, first, we describe the VPP-based posture control in 2D, and then, the extension to 3D will be presented. Finally, the adaptation of the VPP position using anoptimal and robust controller will be explained.

VPP-based Balance control in 2D

As aforementioned, within the VPP concept, balance control is achieved by redirecting the GRF vectors towards a fixed point at each instant of the stance phase. In (Sharbafi et al., 2013), this VPP-based balance control method, called VPPC (virtual pendulum posture control) is presented for the sagittal plane. Using the TSLIP model (see Fig. 1c), the required hip torque (τ) to redirect the GRF to a determined VPP in 2D space is calculated by the following equation:

$$\tau = F_l l \frac{d\sin\psi + r\sin(\psi - \gamma)}{l + d\cos\psi + r\cos(\psi - \gamma)} \quad (2)$$

in which, $F_l, l, r, d, \psi, \gamma$ are the leg force, leg length, the VPP distance to CoM, the hip distance to CoM, the angle between upper-body orientation and the leg, and the VPP's deviation angle from trunk axis, respectively, as shown in Fig. 1c. Here, γ and r are the control parameters which determine the VPP position. Knowing the control parameters γ and r, the required sensory information is the leg force and the angle between the upper body and the leg. These are internal information and no external sensory data (e.g., body orientation with respect to the ground) is required. Further details about this controller are described in (Sharbafi and Seyfarth, 2014).

VPPC in 3D

In this paper, we extend the VPPC method to 3D. According to our experimental results (next section), GRFs intersect below CoM when we look at the sagittal plane, and above CoM when we look at the frontal plane. Based on this observation, our 3D model's upper body is controlled using two separate 2D VPPCs in the sagittal and frontal planes. By combining the corresponding 2D VPPCs, stable running in the 3D model will be achieved (see attached video (S1)). Using indices s, f, and h denoting the corresponding parameters in the sagittal, frontal, and horizontal plane, respectively, the 3D VPPC controller will be given by the following equations:

$$\tau_s = F_{ls} l_s \frac{d_s \sin\psi_s + r_s \sin(\psi_s - \gamma_s)}{l_s + d_s \cos\psi_s + r_s \cos(\psi_s - \gamma_s)}$$
$$\tau_f = F_{lf} l_f \frac{d_f \sin\psi_f + r_f \sin(\psi_f - \gamma_f)}{l_f + d_f \cos\psi_f + r_f \cos(\psi_f - \gamma_f)} \quad (3)$$

It is noteworthy to mention that the two VPP points in the frontal and sagittal planes are not related as they are controlled by different actuators. As a result, the 3D VPPC will be designed by separate adjustment of the VPP positions in the two mentioned planes using the corresponding control parameters (γ and r).

Robust VPPC

As described in (Sharbafi et al., 2013), the VPPC can generate stable running and hopping in 2D. However, to provide robustness against perturbations, the VPP position needs to be adapted. This controller adaptation is also a prerequisite for generating astable and robust running gait in 3D. Inspired by our previous study (Sharbafi et al., 2013), we utilize a linear quadratic regulator (LQR) as an optimal and robust controller to adjust the VPP position once per step. In this higher control level, the new VPP position is computed at each apex (highest CoM height during one step) for the next stance phase (see Fig. 2).

In the coordinate frame shown in Fig. 1d, the 3D template model configuration in the flight phase can be given by the position of CoM and the orientation of the trunk denoted by the kinematic vector $X = [x, y, z, \phi_s, \phi_f, \phi_h]^T$. By detecting the foot contact knowing the attack angle at touchdown, vector X suffices to determine body configuration in the stance phase. Thus, the system state can be defined by $S = [X^T, \dot{X}^T]^T$. Due to the definition of the apex, $\dot{y}$

is equal to zero, and it can be omitted from the state vector. In steady-state running, the horizontal position of the CoM (x) is considered irrelevant and can be omitted. Therefore, the reduced state space at apex will be given by $S = [\dot{x}, y, z, \dot{z}, \phi_s, \dot{\phi}_s, \phi_f, \dot{\phi}_f, \phi_h, \dot{\phi}_h]^T$.

The Poincare return map P between two sequential apex points is defined by $S_{k+1} = P(S_k, U)$, considering the VPP position parameter set $U = [r_s, \gamma_s, r_f, \gamma_f]^T$ as the control input. Assume a fixed VPP position set denoted by U^* creates a periodic 3D running gait. This stable gait can be expressed by the state vector S^* at the apex, as the Poincare map's fixed point. By defining the change of variables $\Delta S_n = (S - S^*)$ and $\Delta U_n = (U - U^*)$, the first order of the Poincare return map around the fixed point S^* can be written as:

$$\Delta S_{n+1} \approx J_S \Delta S_n + J_U \Delta U_n \tag{4}$$

in which, index n indicates the variables in the n^{th} step and $J_S := \frac{\partial P}{\partial S}(S^*, U^*)$ and $J_U := \frac{\partial P}{\partial U}(S^*, U^*)$. By minimizing the following cost function J, the control parameters at each step can be found with the discrete LQR (D-LQR) formulation as an optimal control method (Bertsekas et al., 1995).

$$J = \sum_{k=1}^{\infty} \Delta S_n^T Q \Delta S_n + \Delta U_n^T R \Delta U_n \tag{5}$$

Here, Q and R matrices are weights of error and control effort terms. If the pair (J_S, J_U) is controllable, then ΔS_k can be controlled by the following linear state feedback controller.

$$U_k = -K S_k + U^* \tag{6}$$

Within the D-LQR formulation, the control gain K will be calculated as follows:

$$K = (R + J_U^T P J_U)^{-1} J_U^T P J_S \tag{7}$$

in which, P is the unique positive definite solution of the following discrete time algebraic Riccati equation (kirk, 2004).

$$P = Q + J_S^T (P - P J_U \left(R + J_U^T P J_U\right)^{-1} J_U^T P \right) J_S \tag{8}$$

The importance of the error and energy consumption can be tuned by setting the weighting matrices R and Q.

Swing leg adjustment:

We use the velocity-based swing leg adjustment (VBLA) for calculating the attack angle in the flight phase (Sharbafi and Seyfarth, 2016). This method's advantages in resembling human swing leg movement and providing a robust swing leg adjustment were presented in

(Sharbafi and Seyfarth, 2016). According to the VBLA, the leg direction ($\vec{O}$) is determined by a weighted average of the CoM velocity vector ($\vec{V}$) and the gravity vector ($\vec{G}$). The weight of each vector is decided by a coefficient $0 < \mu < 1$.

$$\vec{O} = \mu \vec{V} + (1 - \mu)\vec{G} \tag{9}$$

in which, $\vec{V} = [v_x, v_y]^T / \sqrt{gl}$ and $\vec{G} = [0, -1]^T$ results in a dimensionless equation. This swing leg placement strategy is used for both sagittal and frontal planes.

RESULTS

This section first investigates the existence of the VPP in human running in the sagittal and frontal planes and the variations concerning gait speed. Then, the simulation results of VPP-based balance control in the 3D running are presented.

VPP in human running

To verify VPP existence at each experimental trial, we found the VPP point as described in the "Experimental data analyses" section and calculated the R^2 value from Eq. (1). As aforementioned, human balance control matches the VPP concept if $R^2 \geq 70\%$. Further, we analyzed the VPP position variation versus running speed.

VPP in sagittal plane

To find the VPP, the GRF vectors are transferred to a CoM-centered coordinate frame that is aligned with the upper body orientation (shown in Fig. 1a). Fig. 3 shows the GRF and the VPP point for one sample running step at $4 m/s$. To remove the impact effect, the GRF data in the first 25% of the stance phase (shown by dashed lines in Fig. 3a) is not considered to calculate the VPP. Fig. 3b depicts the CoM, the VPP, and the GRF vectors (dashed lines) plotted from the CoP in the selected coordinate frame. A clear intersection point at VPP (green circle) is visible in this sample step. In this case, the VPP is placed below the CoM (red circle).

The position of the VPP in the selected coordinate frame and R^2 coefficients are depicted for each step in Fig. 4. Light and dark colors illustrate the corresponding information for the left and right legs, respectively. Except for scarce samples, the VPP position in the sagittal plane is below the CoM for all subjects at different speeds. The coefficient of R^2 for all subjects is higher than 90% , which indicates that the VPP can successfully predict experimental GRFs. Also, there is no significant difference between the right and left legs for the VPP position ($p=0.42$).

The VPP position is not fixed at each speed, but it changes around a line with a negative slope, shown with the same colors used for drawing the VPPs of different legs. The identified regions for the VPP positions at various speeds are comparable (table reftable:VP). The slope of the fitted lines is reduced by increasing the gait speed. On average, the position of the VPP is in front of the CoM at all speeds. This property is also observed in the average CoP position during running gait (see Fig. 3b as an example). More details on the mean and

standard deviation of the VPP location and R^2 values are presented in table .1. On average, the VPP in the sagittal plane is located about $19cm$ below and about $1.2cm$ anteriorto the CoM. Also, horizontal and vertical deviation of the VPP from CoM increases by raising the gait speed except from $4m/s$ to $5m/s$.

VPP in frontal plane

For investigating VPP in the frontal plane, the GRFs are transferred to a CoM-centered coordinate frame aligned based on the pelvis orientation as shown in Fig. 1b. As expected, the VPP positions in thefrontal plane are different for the left and right legs (see two sample steps of running at $4m/s$ in Fig. 5). The focused intersection point of GRFs in Fig. 5 shows that the VPP concept can be extended to the frontal plane by choosing an appropriate coordinate frame. Unlike the sagittal plane, the VPP in the frontal plane is placed above the COM and on the right (left) side of the CoM during the right (left) foot contact. Also, VPP's distance to CoM is not significantly different between the right and left leg (p=0.47).

The VPP positions with R^2 value above 70% are shown in Fig. 6a. The distributions of the VPPs for the left and right steps in the frontal plane are almost symmetric. To quantify this qualitative observation, we depicted the best linear approximation in this figure (dark and light green lines, respectively for right and left leg). Statistical comparison between different speeds is reported in Tab. 1. On average, the VPP in the frontal plane is located about $35cm$ higher than the CoM with about $5cm$ horizontal distance on the same side of the stance foot. To speed up the running gait, the VPP moves downward (towards the CoM) and horizontally farther from the CoM.

Fig. 6b illustrates the R^2 values for both legs of different subjects at four different speeds. Among 80 different cases ($2legs \times 4speeds \times 10subjects$), VPP exists in 70 cases in the frontal plane. The remaining 12.5% of the experimental trials in which VPP was not clearly identified are related to subjects s1, s6, and s7. For s7, clear VPPs with R^2 above 90% (instead of 70%) are found in both legs for all trials except the left leg steps in running at 5m/s. VPPs with R^2 values above 70% can be identified in both legs in most running steps of subject s6 at 2 and $3\ m/s$, and in right leg steps at $4\ m/s$. It is fair to say that s1's running patterns did not show meaningful VPPs in most trials.

In some steps (especially for subject s1), R^2 has a negative value. A negative value for R^2 can be achieved when GRFs are almost parallel. These unacceptable VPPs were not shown in Fig. 6, but the trials experiencing such conditions are illustrated by the pink regions in Fig. 6b. The average R^2 values for all ten subjects are presented in Table. 1. We also calculated the mean R^2 values at each speed without considering subjects s1 and s6, as shown by the colored rows in the table. This new calculation supports the existence of VPP in the frontal plane for eight subjects out of ten.

Simulation result

In this section, we present our simulation results in 3D environments.

The model is able to generate stable running at different speeds. Here we detail the outcomes for running at $4\ m/s$. We set the VPPC control parameter to $r_s = 22cm$ and $\gamma_s = -174^\circ$ for the VPP below CoM in the sagittal plane and $r_f = 30cm$ and $|\gamma_f| = 4^\circ$ for the VPP position above CoM in the frontal plane when the right leg is in the stancephase. Indeed, the sign of γ_f changes by changing the supporting leg (e.g., from right to left) as observed in Fig. 6 for human running. While selecting VPP in the frontal plane, we need to consider the mapping between the model virtual hip and the real hip in humans. For example, by increasing the vertical position of VPP in humans, the horizontal distance from VPP to hip decreases. Therefore, to compensate the increase in r_f in the frontal plane we need to decrease γ_f. Also, we applied a perturbation at the touch-down moment to the CoM speed to investigate the robustness of the system. As stated in the "Robust VPPC" section, event-based control of the VPP position allows us to improve the system behavior and robustness. Controllability of the pair $[J_S, J_U]$ is the only necessary condition easily met in this problem. In addition, using D-LQR for the selection of the gain vector K (Eq. (7)), we can use the weight matrix Q and R in Eq. (5) to determine the importance of the state variables error and control inputs. We set $Q = diag[10,1,1,1,5,1,1,1,1,1]$ to devote higher importance to track the forward speed and trunk angle in the sagittal plane due to the significance of keeping the speed and balance control, especially in confront to the introduced perturbation. Also, the larger weights of the states in the sagittal plane relates to the unstable behavior of the negative VPP (explained in Experiments vs. simulation section). By setting $R = diag[1,1,1,1]$ we equalize the importance of all control inputs.

Fig . 7a shows the trunk angle, forward and medio-lateral speeds of the CoM, besides the VPP parameters (angle and radius), when perturbation occurs in the sagittal plane. Here, perturbation is defined as a sudden 10% increase in the forward speed ($+0.4m/s$). Before applying perturbation, the system is stable, and the model predicts running at $4\ m/s$. Before perturbation, the mean trunk inclination in the sagittal plane is about 5°, and it oscillates between $\pm 4^\circ$ in the frontal plane. After perturbation, the trunk bends backward, and the controller decreases the VPP angle to compensate for perturbation. According to Fig. 7a, there is a clear correlation between the trunk's bending angle and the VPP angle after perturbation. The perturbation in the sagittal plane also affects trunk orientation in the frontal plane due to the coupling between two planes. By changing the VPP parameters to cover from perturbation, the D-LQR controller can stabilize the system after a few steps, and system states converge to the states before perturbation.

The robustness of the system against lateral perturbation is investigated by examining the reaction of the VPPC to a sudden increase in the medio-lateral speed (100% of maximum medio-lateral speed is added ($+0.05m/s$)). Fig. 7b demonstrates that the perturbation has a negligible impact on the forward speed and trunk angle in the frontal plane, while the medio-lateral speed and the trunk angle in the sagittal plane need a few steps for recovery.

DISCUSSION

We selected the VPP concept to analyze postural stability in running in a 3D space. The quality of the identified VPP is utilized as a measure to evaluate the VPP method in predicting human running. Moreover, replicating the experimental results in a template-based

simulation model confirmed the proposed method's functionality. In addition to discussing the presented outcomes, a detailed comparison between simulation and human running is presented in the following.

VPP quality and location in human gait

Previous studies reveal that appropriate control of whole-body angular momentum (WBAM) is critical to maintaining dynamic balance during locomotion (Begue et al., 2019). The WBAM can be computed by integrating the net external moment produced by the measured ground reaction forces around the CoM. Experimental evidence shows that the WBAM remains small during steady-state human walking (Herr and Popovic, 2008). Further, the prediction ability of the WBAM regulation decreases as the locomotion task becomes more dynamic (from standing and walking to running) (Popovic et al., 2002). As a more general postural control measure, the VPP concept not only can predict WBAM variations (Gruben and Boehm, 2012) but also can describe human balance control in more dynamic locomotion tasks. In this regard, we analyzed human running and the identified VPP in the sagittal and frontal planes at different speeds.

VPP in sagittal plane: As stated in the "METHODS" section, the R^2 value indicates the amount of agreement between experimentally measured GRFs and force vectors predicted by the VPP method. The distinguished VPP (R^2 about 98%) in the sagittal plane demonstrates the remarkable matching of the experimental measurements and the predicted posture control. Similar high R^2 values are reported by Drama et al. at 5m/s level ground running (Drama et al., 2020). Here, the VPP is placed below CoM (negative VPP) at all speeds (except in scarce samples), which means the WBAM component in the sagittal plane has a negative mean value. This result is in line with the previous findings showing the WBAM drops in the first half of the stancephase and raises in the second half of the stance phase (Sepp et al., 2019; Hinrichs, 1987). Also, our results confirm the negative VPP found in (Drama et al., 2020). The negative VPP creates GRFs passing behind the CoM in the first half of the stance phase, exerting a flexion moment on the body, which causes the drop in the WBAM. The subsequent rise in the WBAM during the second half of the stance phase resultsfrom the GRF vectors passing the negative VPP and, consequently, in front of the CoM (Hinrichs, 1987). The negative VPP increases the acceleration and deceleration in the fore-aft direction compared to the positive VPP, observed in human walking (Drama and Badri-Spröwitz, 2019; Maus et al., 2010). Furthermore, a simulation study shows that the negative VPP reduces the leg loading and net hip work (Drama and Badri-Spröwitz, 2019).

The experimental data (Table .1) shows that VPP in the sagittal plane is located anterior to the CoM at all speeds ($p<0.001$). This observation can be explained using the trunk inclination and the WBAM behavior in the sagittal plane. Since thenet external moment acting on the CoM in the flight phase is zero, the WBAM remains constant. Hence, for a periodic motion such as running (considering left and right leg symmetry in the sagittal plane), it is necessary to create a restoring extension moment in the second half of the stance phase to compensate for the flexion moment in the first half of the stance phase. In other words, the external moment resulted from the GRF must become balanced around the CoM (Fig. 3). The counterbalance results in forward inclination of the upper-body.

The horizontal deviation of the VPP from CoM increases with running speed as a faster gait needs a more inclined trunk. In addition to increasing upper-body inclination, distancing VPP from CoM could increase both braking and propulsive forces. To further analyze the connection between the VPP position and the gait speed, the general trend of calculated VPPs was approximated by a linear relation. As shown in Fig. 4 and Table .1, the faster the running, the higher the slope of the fitted line. This means that for faster motions, the horizontal adjustment of the VPP is employed more than the vertical adjustment and vice versa.

VPP in frontal plane: The WBAM in the frontal plane has a greater range than sagittal and horizontal planes during running (Sepp et al., 2019; Hinrichs, 1987). According to Table .1, the mean R^2 value of the VPP in the frontal plane is about 80% , meaning that the VPP concept is also valid for analyzing lateral balancing. The existence of the VPP cannot be verified for two out of ten subjects. Skipping these two subjects' data, the average R^2 will be about 90% which certifies VPP-based lateral balance control for 80% of the dataset. Unlike the sagittal plane, positive VPP (above CoM) is found in the frontal plane, at all speeds, except for sporadic samples. Also, the VPP is placed on the same side of the CoM that the support leg is. Compared to the CMP (centroidal moment pivot) (Herr and Popovic, 2008), this feature of VPP placement helps better predict the WBAM and balance external momentum around the CoM at each gait cycle in the frontal plane (Hinrichs, 1987). The WBAM in the frontal plane raises when the left leg is in contact with the ground and drops when the right leg is in contact with the ground. In other words, the runner's body axis always tends to lean toward the swing leg. It seems that the VPP position could compromise between hip torque minimization and WBAM minimization.

By increasing the speed up to $4m/s$, the VPP tends to move towards the stance leg hip joint (equivalently, increasing distance from COM). This pattern in VPP placement is observed in speeds up to the preferred running speed ($4m/s$ as stated in (Kong et al., 2012)). Thus, from slow to moderate running, the priority of hip abduction torque minimization is higher than WBAM minimization. However, a faster gait enforces a shorter step duration, and as a result, the increase in WBAM does not yield higher upper body inclination. Roughly speaking, tuning the distance between VPP and CoM can be used to control the WBAM by adjusting the lever arm of the GRF around the CoM. Therefore, the upper body keeps balance by fast switching between two unstable modes (tend to fall toward the swing leg) (Firouzi et al., 2019). Finally, increasing the horizontal distance between the VPP and the body's CoM decreases the lever arm of the GRF around the knee joint center in the frontal plane and consequently reduces the varus moment. This may be a mechanism to reduce injury risk during running (Powers, 2010).

Experiments vs. simulation

The VPP below CoM (negative VPP), found in human experiments in the sagittal plane, represents an inverted pendulum behavior that is inherently unstable (Firouzi et al., 2019; Muller et al., 2017). Therefore, such a negative VPP is not robust against even small perturbation except using an adaptation method (e.g., D-LQR). This finding is supported by the simulation results (Fig .7), showing that the perturbation impact on the trunk angle is more significant in the sagittal plane than in the frontal plane. In this study, we used perturbation to investigate the robustness of our simulation when the position of VPP is considered as a control target. If the VPP is the key for balance control, it should also have a

solution for perturbation recovery. Our simulation results show that the 3D model can easily recover from perturbation using VPP position readjustment. These results are in line with the Drama et al. finding that VPP's horizontal position in level running differs from that of perturbed running (Drama et al., 2020). This observation also reveals the potential of VPP adjustment to be used in robot posture control.

The simulation results showed that for stable running with a slightly inclined trunk, the VPP should be placed anterior to the CoM, which complies with the experimental results. Furthermore, to recover from the perturbation, the VPP shifts backward (in the selected coordinate frame), which decreases the trunk inclination (Fig. 7a).

We used the previously mentioned 3D running simulations at $4 m/s$ to further validate the ability of the VPP concept and the proposed model in predicting human balance control and mimicking human running kinematic and kinetic behavior. First column of Fig. 8 shows the trunk angle in the sagittal and frontal plane for simulations and experiments. The mean trunk inclination in the sagittal plane for experimental data is nicely matching to our simulation results. However, the simulated trunk angle pattern differs from the measured angle patterns at the beginning of the stance phase. The observed forward movement in the early stance phase which is also consistent with the previous studies (Thorstensson et al., 1984) is resulted from the negative VPP. The difference between simulation and experiment results from the swing phase modeling imprecision; as in our template model, the swing phase is represented by a ballistic motion considering a constant angular velocity of the trunk. On the contrary, the human trunk moves backward in the first half of the swing phase, followed by a forward movement. It is important to say that the human-like trunk movement in the stance phase is replicated by the model with a short delay, which is required to compensate for the missing trunk movement in the previous swing phase. One way to improve the similarity between the model and the human experiment is to add mass to the leg of our template model as implemented in the XTSLIP model presented in (Sharbafi et al., 2013). The trunk lateral angle (in the frontal plane) of the simulation model resembled the experimental data in the stance phase. Also, the mean pelvis inclination in the stance phase is quite similar for experiment and simulation. The XTSLIP model may also predict upper body returning movement in the flight phase, which is missing in our model.

The second column of Fig. 8 shows the hip torque in the sagittal (extension/flexion) and frontal (abduction/adduction) planes for both simulations and experiments. In human running, the stance phase starts with a small (negative) flexionhip torque followed by a large extension torque to support the desired forward movement of the body. The model predicts a larger hip flexion than what was found in the experiment to compensate for the swing phase movement. Then, the forward motion is generated by an extension torque which is larger and longer than the preceding flexion torque (similar to the experiment). Since our model can control the trunk angle only in the stance phase, the hip joint first needs to resist the trunk's backward motion and then compensate for flexion torque exerted by the trunk weight. The simulation model can predict the hip adduction torque (in the frontal plane) in the stance phase.

Limitation of this study

In this study, we skipped the data at the first 25% of the stance phase to remove the impact effect. Impact duration, differ among directions and foot strike conditions. For example, the impact phase duration varies from 15% to 30% of the stance phase due to the running style

(e.g., fore-foot strike, heel-strike or heel-toe running) (Nordin et al., 2017). In our dataset most of the subjects identified as mid-foot to heel-strike runners which show longer impact duration (for more information see (Hamner and Delp, 2013)). The impact effect might be compensated by intrinsic compliant element behaviour in the leg which does not undervalue the VPP-based posture control in most of the stance period. This limitation of this study can be further investigated in the future.

Moreover, we used an existing data set (collected by another research group) that did not include women. Although the VPP concept is observed in both women and men locomotion in the previous studies (Gruben and Boehm, 2012; Drama et al., 2020), excluding women in this study is a limitation that needs to be addressed in future studies.

Conclusion

In this study, we investigated the virtual pivot point (VPP) in human running gait at a range of speeds in both sagittal and frontal planes, and analyzed the implication of the observed VPP to balance control using a 3D template model. Our findings show that ground reaction forces intersect near a point below CoM in the sagittal plane and above the CoM in the frontal plane at all speeds. Also, replicating the kinematic and kinetic behavior of the experiments with the template-based simulation model supports the applicability of the VPP concept in predicting human posture control in running. Further, we showed that VPP adaptation at each step (e.g., using a D-LQR) can stabilize the gait and warrants the robustness against perturbations. Our synthesizing method can be used for developing model-based control approaches in humanoid robots and for gait assistance.

APPENDIX

3D template equation of motion:

The 3D model introduced in the "METHODS" section and the VPPC controller are described in this section. Let's define the CoM position by (x, y, z) and the trunk angles in the sagittal, frontal, and horizontal planes, respectively by ϕ_s, ϕ_f, and ϕ_h. The model shown in Fig. 1d can be formulated by the following equations:

$$
\begin{aligned}
&\text{Stance}: \begin{cases}
m\ddot{x} = GRF_x \\
m\ddot{y} = GRF_y - mg \\
m\ddot{z} = GRF_z \\
J_s\ddot{\phi}_s = \tau_s + d_s\left(GRF_x sin\phi_s - GRF_y cos\phi_s\right) \\
J_f\ddot{\phi}_f = \tau_f + d_f\left(GRF_z sin\phi_f - GRF_y cos\phi_f\right) \\
J_h\ddot{\phi}_h = \left(\left(x_h - x_f\right) + d_s cos\left(\phi_s\right)\right)GRF_z \ldots \\
-\left(\left(z_h - z_f\right) + d_f cos\left(\phi_f\right)\right)GRF_x
\end{cases} \\
&\text{Flight}: \begin{cases}
\ddot{x} = 0 \\
\ddot{y} = -g \\
\ddot{z} = 0 \\
\ddot{\phi}_s = 0 \\
\ddot{\phi}_f = 0 \\
\ddot{\phi}_h = 0
\end{cases}
\end{aligned}
\tag{10}
$$

The parameters of this model are described in Tab. 2. In Eq. (10), the ground reaction forces are:

$$
\begin{aligned}
GRF_x &= F_{ls}\frac{x_h - x_f}{l_s} + \tau_s\frac{y_h}{l_s^2} \\
GRF_y &= F_{ls}\frac{y_h}{l_s} - \tau_s\frac{x_h - x_f}{l_s^2} - \tau_f\frac{z_h - z_f}{l_f^2} \\
GRF_z &= F_{lf}\frac{z_h - z_f}{l_f} + \tau_f\frac{y_h}{l_f^2}
\end{aligned}
\tag{11}
$$

in which the hip position is defined as follows

$$
\begin{aligned}
x_h &= x - d_s cos\phi_s \\
y_h &= y - d_s sin\phi_s \\
z_h &= z - d_f cos\phi_f
\end{aligned}
\tag{12}
$$

Further, the leg force f_l is the produced force by the leg spring and damper. We use a bilinear damper as a more realistic model of the leg damping behavior in running, as described in (Abraham et al., 2015).

$$
F_l = k\left(l_0 - l\right) - c\dot{l}\left(l_0 - l\right) \tag{13}
$$

Acknowledgements
We are thankful for the constructive discussions with Andre Seyfarth on the description of the results. The authors also thank Omid Mohseni for his support in revising the paper.

Competing interests
The authors have declared no competing interest.

funding
This research was partially supported by the DFG (German Science Foundation) funded EPA and EPA-2 projects, under the grant numbers AH307/2–1 and AH307/4-1, respectively.

Data availability
Experimental data of the human running experiments is from (Hamner et al., 2010) and freely available at https://simtk.org/projects/nmbl_running.

supplementary
S1: A video of running performance with the proposed 3D model.

REFERENCES

Kim, S. & Wensing, P. Design of dynamic legged robots. *Foundations And Trends In Robotics*. **5**, 117-190 (2017)

Blickhan, R. The spring-mass model for running and hopping. *Journal Of Biomechanics*. **22**, 1217-1227 (1989)

Ahmadi, M. & Buehler, M. The ARL monopod II running robot: control and energetics. *Proceedings 1999 IEEE International Conference On Robotics And Automation (Cat. No.99CH36288C)*. **3** pp. 1689-1694 vol.3 (1999)

Hubicki, C., Grimes, J., Jones, M., Renjewski, D., Spröwitz, A., Abate, A. & Hurst, J. Atrias: Design and validation of a tether-free 3d-capable spring-mass bipedal robot. *The International Journal Of Robotics Research*. **35**, 1497-1521 (2016)

Seok, S., Wang, A., Chuah, M., Hyun, D., Lee, J., Otten, D., Lang, J. & Kim, S. Design principles for energy-efficient legged locomotion and implementation on the MIT cheetah robot. *Ieee/asme Transactions On Mechatronics*. **20**, 1117-1129 (2014)

Tajima, R., Honda, D. & Suga, K. Fast running experiments involving a humanoid robot. *2009 IEEE International Conference On Robotics And Automation*. pp. 1571-1576 (2009)

Sharbafi, M., Lee, D., Kiemel, T. & Seyfarth, A. Fundamental Subfunctions of Locomotion. *Bioinspired Legged Locomotion*. pp. 11-53 (2017)

Thorstensson, A., Nilsson, J., Carlson, H. & ZOMLEFER, M. Trunk movements in human locomotion. *Acta Physiologica Scandinavica*. **121**, 9-22 (1984)

Drama, Ö. & Badri-Spröwitz, A. Trunk pitch oscillations for joint load redistribution in humans and humanoid robots. *2019 IEEE-RAS 19th International Conference On Humanoid Robots (Humanoids)*. pp. 531-536 (2019)

Bramble, D. & Lieberman, D. Endurance running and the evolution of Homo. *Nature*. **432**, 345-352 (2004)

Sharbafi, M., Rode, C., Kurowski, S., Scholz, D., Möckel, R., Radkhah, K., Zhao, G., Rashty, A., Stryk, O. & Seyfarth, A. A new biarticular actuator design facilitates control of leg function in BioBiped3. *Bioinspiration & Biomimetics*. **11**, 046003 (2016)

Nasiri, R., Ahmadi, A. & Ahmadabadi, M. Reducing the energy cost of human running using an unpowered exoskeleton. *IEEE Transactions On Neural Systems And Rehabilitation Engineering*. 26, 2026-2032 (2018)

Sugar, T., Fernandez, E., Kinney, D., Hollander, K. & Redkar, S. HeSA, hip exoskeleton for superior assistance. *Wearable Robotics: Challenges And Trends*. pp. 319-323 (2017)

Zhao, G., Sharbafi, M., Vlutters, M., Asseldonk, E. & Seyfarth, A. Bio-Inspired Balance Control Assistance Can Reduce Metabolic Energy Consumption in Human Walking. *IEEE Transactions On Neural Systems And Rehabilitation Engineering*. **27**, 1760-1769 (2019)

Popovic, M., Goswami, A. & Herr, H. Ground reference points in legged locomotion: Definitions, biological trajectories and control implications. *The International Journal Of Robotics Research*. **24**, 1013-1032 (2005)

Kajita, S., Nagasaki, T., Kaneko, K. & Hirukawa, H. ZMP-Based Biped Running Control. *IEEE Robotics Automation Magazine*. **14**, 63-72 (2007)

Goswami, A. Postural stability of biped robots and the foot-rotation indicator (FRI) point. *The International Journal Of Robotics Research*. **18**, 523-533 (1999)

Maus, H., Lipfert, S., Gross, M., Rummel, J. & Seyfarth, A. Upright human gait did not provide a major mechanical challenge for our ancestors. *Nature Communications*. **1** pp. 70 (2010)

Peekema, A. Template-based control of the bipedal robot atrias. (2015)

Zhao, G., Sharbafi, M., Vlutters, M., Van Asseldonk, E. & Seyfarth, A. Template model inspired leg force feedback based control can assist human walking. *2017 International Conference On Rehabilitation Robotics (ICORR)*. pp. 473-478 (2017)

Firouzi, V., Davoodi, A., Bahrami, F. & Sharbafi, M. From a biological template model to gait assistance with an exosuit. *Bioinspiration & Biomimetics*. (2021)

Sharbafi, M., Ahmadabadi, M., Yazdanpanah, M., Nejad, A. & Seyfarth, A. Compliant hip function simplifies control for hopping and running. *2013 IEEE/RSJ International Conference On Intelligent Robots And Systems*. pp. 5127-5133 (2013)

Blickhan, R., Andrada, E., Müller, R., Rode, C. & Ogihara, N. Positioning the hip with respect to the COM: consequences for leg operation. *Journal Of Theoretical Biology*. 382 pp. 187-197 (2015)

Drama, Ö., Vielemeyer, J., Badri-Spröwitz, A. & Müller, R. Postural stability in human running with step-down perturbations: an experimental and numerical study. *Royal Society Open Science*. **7**, 200570 (2020)

Kuo, A. Stabilization of lateral motion in passive dynamic walking. *The International Journal Of Robotics Research*. **18**, 917-930 (1999)

Arellano, C. & Kram, R. The effects of step width and arm swing on energetic cost and lateral balance during running. *Journal Of Biomechanics*. **44**, 1291-1295 (2011)

Krebs, D., Goldvasser, D., Lockert, J., Portney, L. & Gill-Body, K. Is base of support greater in unsteady gait?. *Physical Therapy*. **82**, 138-147 (2002)

MacKinnon, C. & Winter, D. Control of whole body balance in the frontal plane during human walking. *Journal Of Biomechanics*. **26**, 633-644 (1993)

Hamner, S. & Delp, S. Muscle contributions to fore-aft and vertical body mass center accelerations over a range of running speeds. *Journal Of Biomechanics*. **46**, 780-787 (2013)

Hamner, S. & Delp, S. 'Muscle contributions to mass center accelerations over a range of running speeds'. ([Online]. Available: https://simtk.org/projects/nmbl_running. [Accessed: 19-March-2019].,0)

Hamner, S., Seth, A. & Delp, S. Muscle contributions to propulsion and support during running. *Journal Of Biomechanics*. **43**, 2709-2716 (2010)

Delp, S., Anderson, F., Arnold, A., Loan, P., Habib, A., John, C., Guendelman, E. & Thelen, D. OpenSim: open-source software to create and analyze dynamic simulations of movement. *IEEE Transactions On Biomedical Engineering*. **54**, 1940-1950 (2007)

Vielemeyer, J., Grießbach, E. & Müller, R. Ground reaction forces intersect above the center of mass even when walking down visible and camouflaged curbs. *Journal Of Experimental Biology*. **222**, jeb204305 (2019)

Herr, H. & Popovic, M. Angular momentum in human walking. *Journal Of Experimental Biology*. **211**, 467-481 (2008)

Firouzi, V., Seyfarth, A. & Sharbafi, M. TIP Model: A Combination of Unstable Subsystems for Lateral Balance in Walking. *2019 IEEE/RSJ International Conference On Intelligent Robots And Systems (IROS)*. pp. 476-482 (2019)

Sharbafi, M. & Seyfarth, A. Stable running by leg force-modulated hip stiffness. *5th IEEE RAS/EMBS International Conference On Biomedical Robotics And Biomechatronics*. pp. 204-210(2014)

Sharbafi, M., Maufroy, C., Ahmadabadi, M., Yazdanpanah, M. & Seyfarth, A. Robust hopping based on virtual pendulum posture control. *Bioinspiration & Biomimetics*. **8**, 036002 (2013)

Maus, H., Rummel, J. & Seyfarth, A. Stable upright walking and running using a simple pendulum based control scheme. *International Conference Of Climbing And Walking Robots*. pp. 623-629 (2008)

Bertsekas, D., Bertsekas, D., Bertsekas, D. & Bertsekas, D. Dynamic programming and optimal control. (Athena scientific Belmont, MA,1995)

Kirk, D. Optimal control theory: an introduction. (Courier Corporation,2004)

Sharbafi, M. & Seyfarth, A. VBLA, a swing leg control approach for humans and robots. *2016 IEEE-RAS 16th International Conference On Humanoid Robots (Humanoids)*. pp. 952-957 (2016)

Kong, P., Koh, T., Tan, W. & Wang, Y. Unmatched perception of speed when running overground and on a treadmill. *Gait & Posture*. **36**, 46-48 (2012), https://www.sciencedirect.com/science/article/pii/S0966636212000021

Begue, J., Peyrot, N., Dalleau, G. & Caderby, T. Age-related changes in the control of whole-body angular momentum during stepping. *Experimental Gerontology*. **127** pp. 110714 (2019)

Popovic, M., Gu, W. & Herr, H. Conservation of angular momentum during human locomotion. *MIT, Artificial Intelligence Laboratory, Research Abstracts. September*. **231** pp. 232(2002)

Gruben, K. & Boehm, W. Force direction pattern stabilizes sagittal plane mechanics of human walking. *Human Movement Science*. **31**, 649-659 (2012)

Sepp, L., Baum, B., Nelson-Wong, E. & Silverman, A. Dynamic balance during running using running-specific prostheses. *Journal Of Biomechanics*. **84** pp. 36-45 (2019)

Hinrichs, R. Upper extremity function in running. II: Angular momentum considerations. *Journal Of Applied Biomechanics*. **3**, 242-263 (1987)

Powers, C. The influence of abnormal hip mechanics on knee injury: a biomechanical perspective. *Journal Of Orthopaedic & Sports Physical Therapy*. **40**, 42-51 (2010)

Müller, R., Rode, C., Aminiaghdam, S., Vielemeyer, J. & Blickhan, R. Force direction patterns promote whole body stability even in hip-flexed walking, but not upper body stability in human upright walking. *Proceedings Of The Royal Society A: Mathematical, Physical And Engineering Sciences*. **473**, 20170404 (2017)

Abraham, I., Shen, Z. & Seipel, J. A nonlinear leg damping model for the prediction of running forces and stability. *Journal Of Computational And Nonlinear Dynamics*. **10** (2015)

Budday, D., Bauer, F. & Seipel, J. Stability and robustness of a 3D SLIP model for walking using lateral leg placement control. *ASME 2012 International Design Engineering Technical Conferences And Computers And Information In Engineering Conference*. pp. 859-866 (2012)

McMahon, T. & Cheng, G. The mechanics of running: how does stiffness couple with speed?. *Journal Of Biomechanics*. **23** pp. 65-78 (1990)

Seipel, J. & Holmes, P. Three-dimensional running is unstable but easily stabilized. *Climbing And Walking Robots*. pp. 585-592 (2005)

Sharbafi, M. & Seyfarth, A. FMCH: A new model for human-like postural control in walking. *Intelligent Robots And Systems (IROS), 2015 IEEE/RSJ International Conference On*. pp. 5742-5747 (2015)

Nordin, A., Dufek, J. & Mercer, J. Three-dimensional impact kinetics with foot-strike manipulations during running. *Journal Of Sport And Health Science*. **6**, 489-497 (2017)

Damavandi, M., Stylianides, G., Farahpour, N. & Allard, P. Head and trunk segment moments of inertia estimation using angular momentum technique: Validity and sensitivity analysis. *IEEE Transactions On Biomedical Engineering*. **58**, 1278-1285 (2010)

Figures

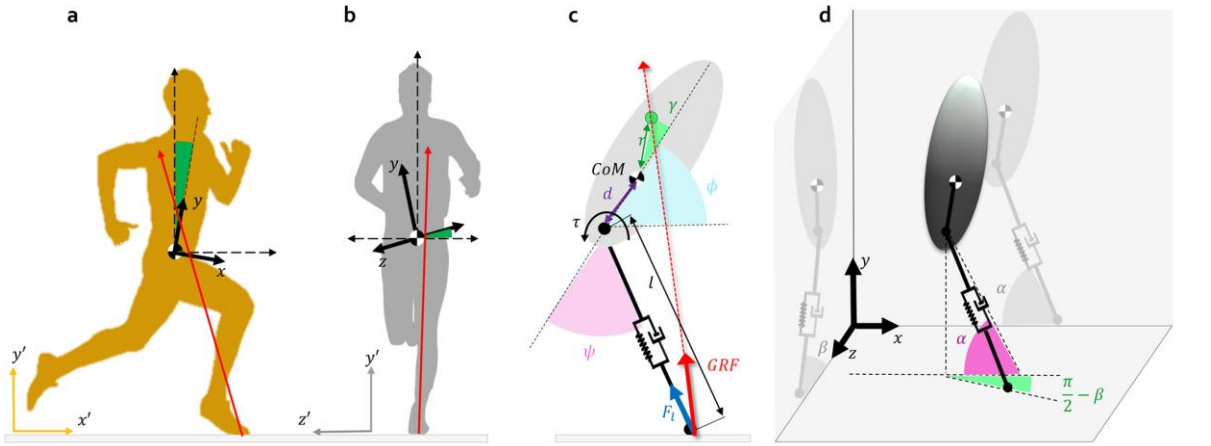

Figure 1. a) Selected reference frame (x, y) for analyzing the VPP in the sagittal plane. The upper body orientation defines the vertical (y) axis. b) Selected reference frame (z, y) for analyzing the VPP in the frontal plane. The pelvis orientation defines the horizontal (z) axis. The whole body CoM is selected as the origin of these frame. The world reference frame is shown by (x', y', z'). c) 2D template model with a rigid trunk and a massless spring-damper for the leg. The required variables and parameters to derive equation of motion are shown. The green circle depicts the VPP and its distance to the CoM and the angle to the trunk orientation are illustrated with green color. d) The 3D extended model and its 2D projections in the frontal and sagittal planes. α and β are the attack angles in the sagittal and frontal planes, respectively.

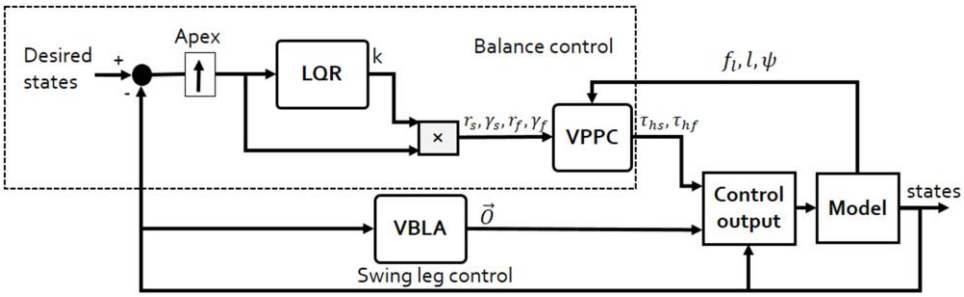

Figure 2. Illustration of our control method. Balance control block gives hip torque τ during stance. the VPPC block calculates hip torque for a fixed VPP. At each apex, LQR controller adapts VPP position. Swing leg control calculates swing leg angle of attack.

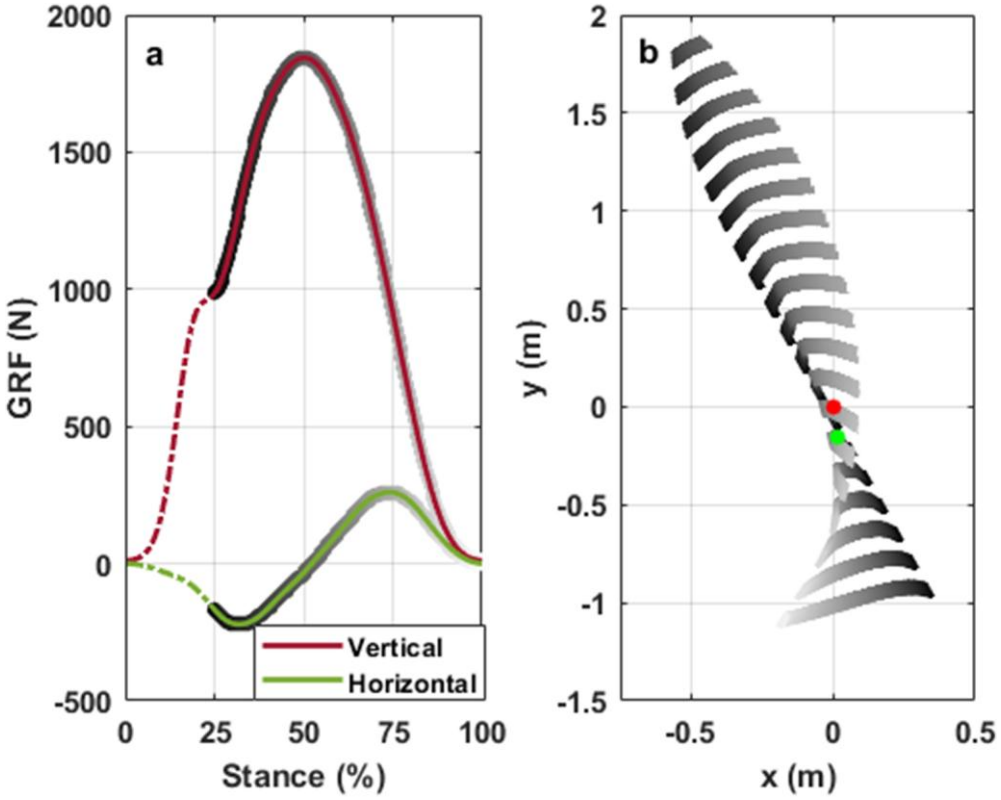

Figure 3. Ground reaction force (GRF) and VPP in the sagittal plane of a sample human running step at 4 m/s. a) GRF magnitudes in the vertical and horizontal (anterior-posterior) directions. The data from the first 25% of the stance phase (shown with dashed lines) are skipped in VPP calculation to remove the impact effect. b) Demonstration of VPP existence (green circle). GRF vectors are plotted with dashed lines from the CoP in the coordinate frame centered atCoM (red circle) and aligned with upper-body orientation.

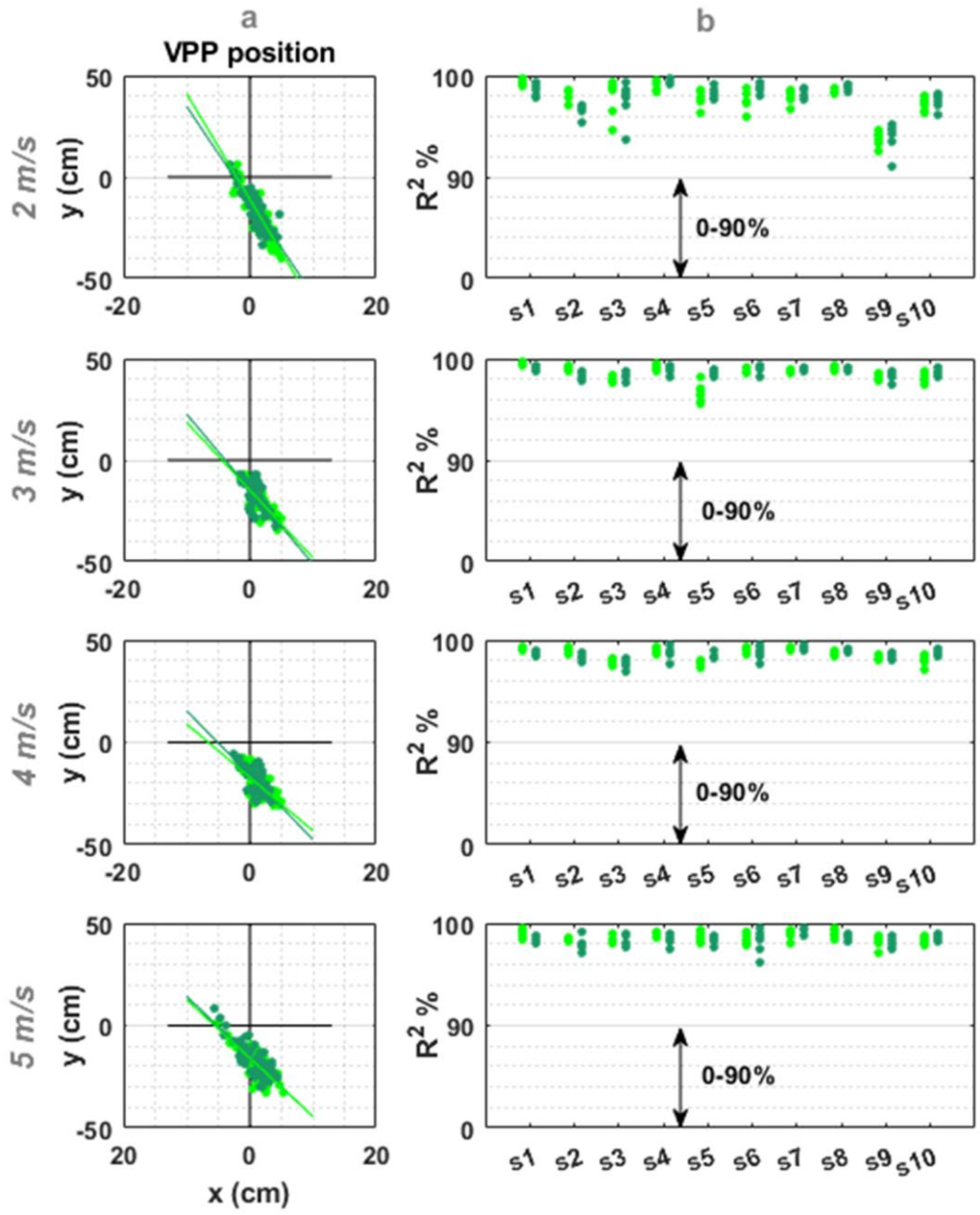

Figure 4. VPP existence in the sagittal plane. The results are shown in different colors for the right and left legs. a) Calculated VPP positions from ten subjects (s1 to s10) running at different speeds. b) R^2 coefficients calculated for VPP at each step.

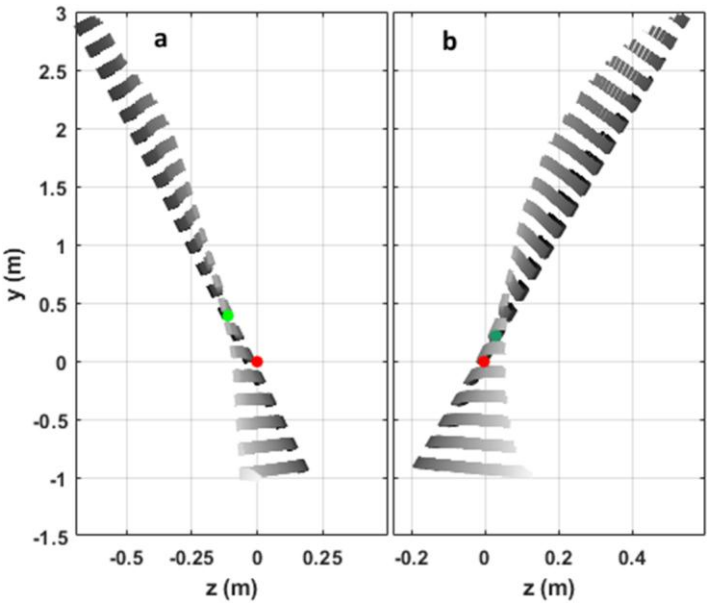

Figure 5. Example of ground reaction vectors and the calculated VPP in the frontal plane of human running experiment. GRFs are plotted with respect to a CoM-centered, pelvis coordinate frame. Green and red circles show VPP and CoM, respectively. a) Left leg. b) Right leg.

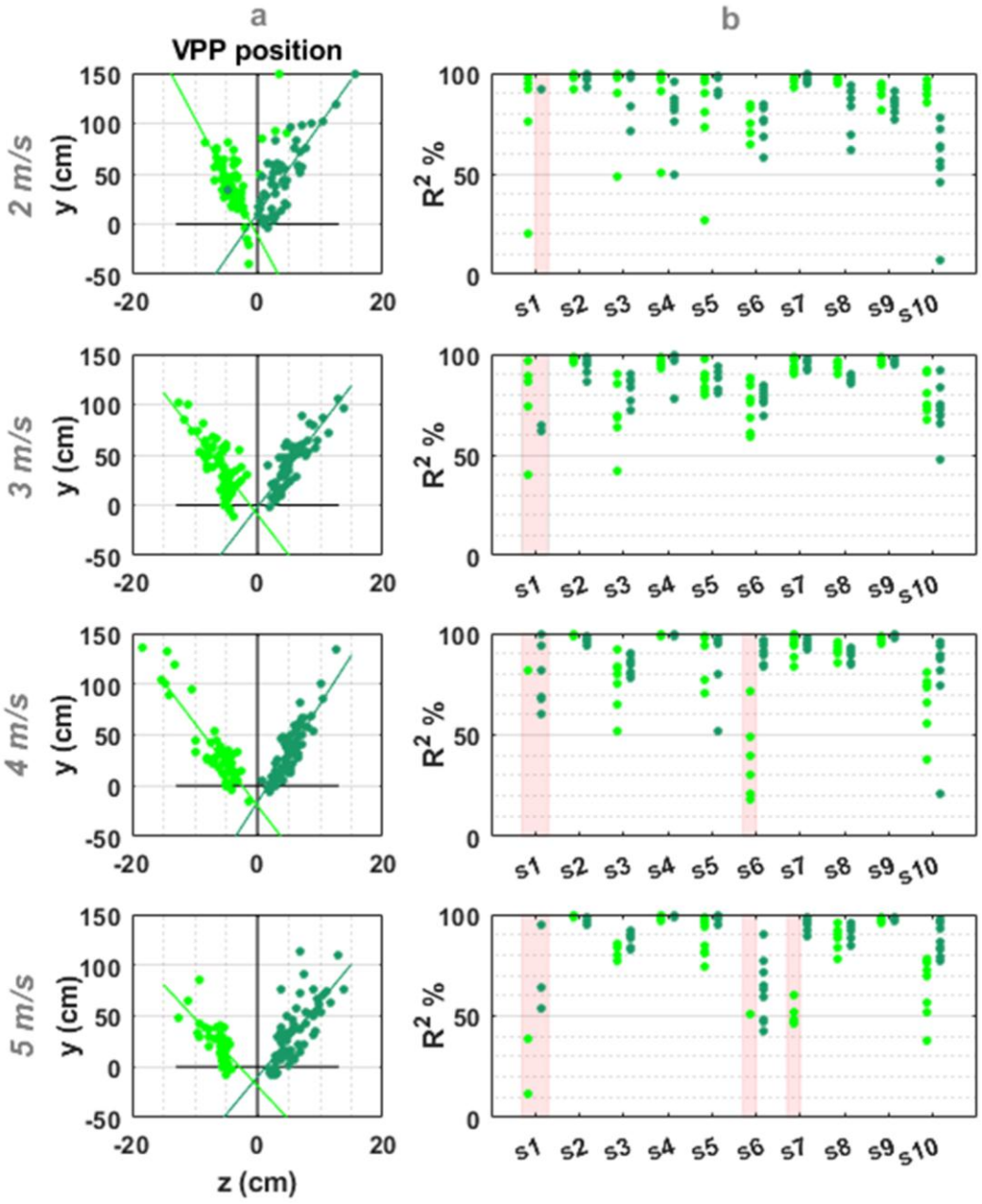

Figure 6. VPP existence in frontal plane. The results are shown in different colors for the right and left legs. a) Calculated VPP positions from ten subjects (s1 to s10) running at different speeds. b) R^2 coefficients calculated for VPP at each step. The shadowed pink boxes represent the cases with unacceptable (e.g., negative) R^2 values meaning VPP is not found.

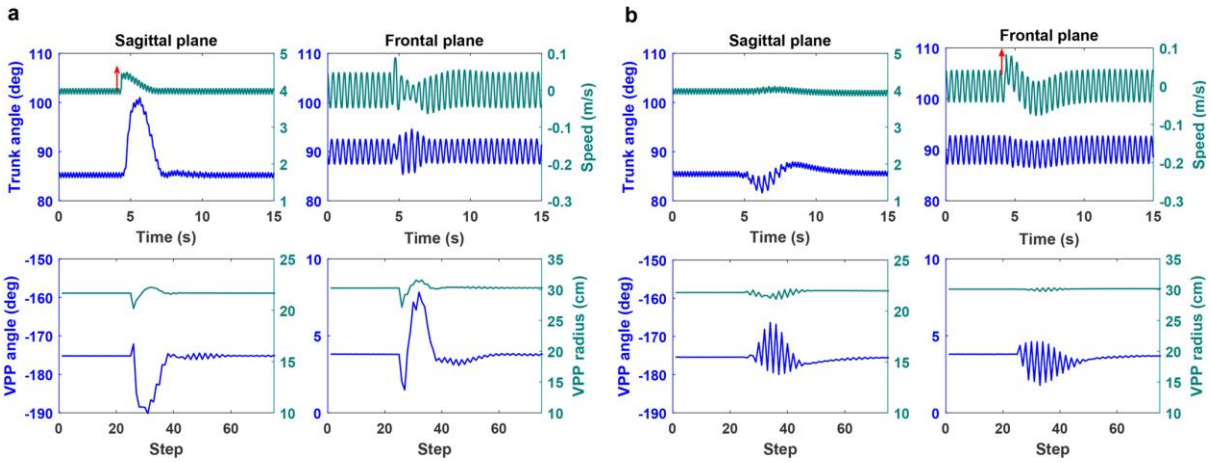

Figure 7. Simulation results of 3D running at $4\ m/s$. The graphs show the performance and control variations in the sagittal and frontal planes. The first row depicts the trunk angle and the CoM speed as important system states, and the second row showsVPP control variables. a) With perturbation in forward speed (10% increase ($+0.4 m/s$)). b) With perturbation in the medio-lateral speed (100% of the maximum medio-lateral speed is added ($+0.05 m/s$)). The perturbation has been applied at the touch-down moment, and has been shown by the red arrow.

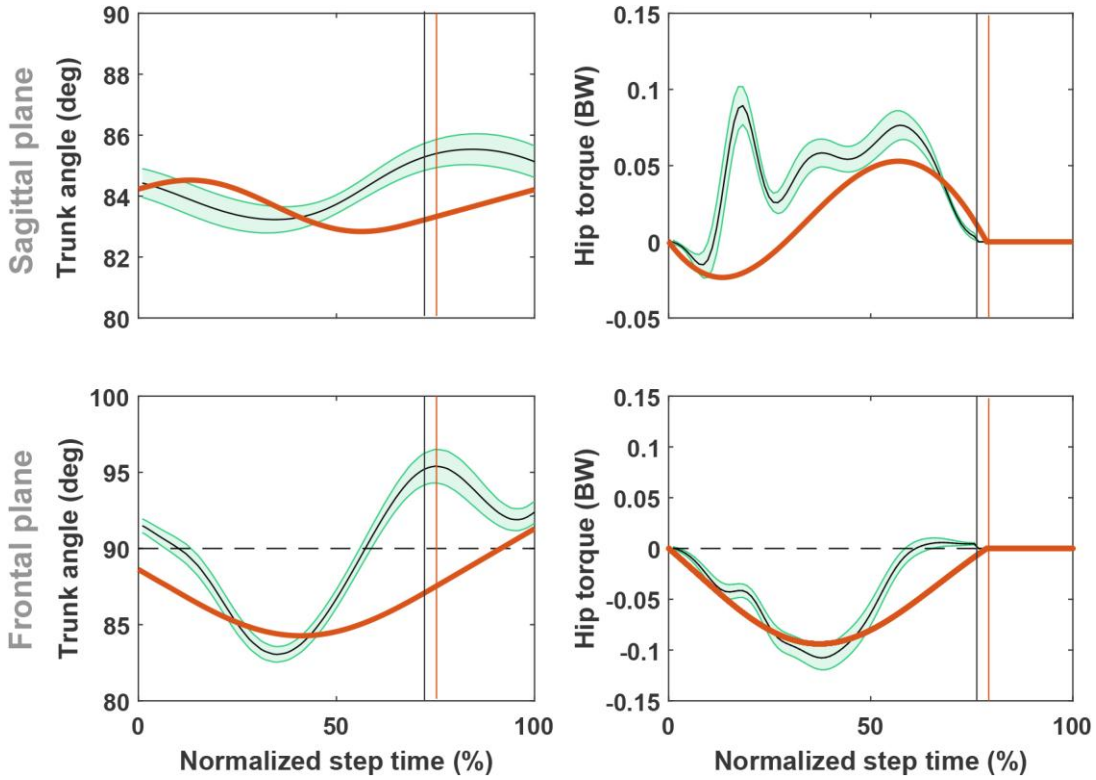

Figure 8. Comparison of trunk angle (first column) and hip torque (second column) in the sagittal and frontal plane for experiment and simulation. Solid curve and curve with the shaded region show simulation and experiment, respectively. the vertical line shows the toe-off moment.

Table 1. Mean ± STD value for VPP variables (location and R^2 value). Colored rows in the table show the mean R2 values at each speed, without considering subjects $s1$ and $s6$. Significant differences from 2 m/s, 3 m/s and 4 m/s running are indicated with 'a', 'b', and 'c', respectively ($p < 0.05$). For statistical analysis, we used repeated measures ANOVAs with post hoc analysis and speed as the factor.

Plane	VPP variables	2 m/s	3 m/s	4 m/s	5 m/s
Sagittal	$VPP_{yR}\,(cm)$	-16 ± 8.6	-18.7 ± 6.5^{a}	-20 ± 6.1^{a}	-18 ± 7.3
	$VPP_{xR}\,(cm)$	0.86 ± 1.6	1.2 ± 1.3	1.38 ± 1.4^{a}	1.1 ± 2
	$VPP_{yL}\,(cm)$	-17 ± 11.6	-20 ± 6.2	-21.5 ± 5.8^{a}	-19.5 ± 6.8
	$VPP_{xL}\,(cm)$	1 ± 3	1.6 ± 1.4	1.7 ± 1.5	1.3 ± 1.7
	linear fit ($y_R = ax_R + b$)	$-4.65x - 12$	$-3.7x - 14$	$-3.14x - 16$	$-2.9x - 15$
	linear fit ($y_L = ax_L + b$)	$-5.2x - 10$	$-3.34x - 15$	$-2.6x - 17$	$-2.8x - 16$
	$R_R^2\,(\%)$	96.8 ± 1.6	98.7 ± 0.4	98.6 ± 0.5	98.5 ± 0.6
	$R_R^2\,(\%)$	97.1 ± 1.2	98.6 ± 0.5	99 ± 0.5	98.8 ± 0.6
	$R_L^2\,(\%)$	97.7 ± 2	98.5 ± 0.8	98.6 ± 0.6	98.6 ± 0.5
	$R_L^2\,(\%)$	98 ± 1.5	98.2 ± 0.6	98.8 ± 0.8	98.6 ± 0.5
Frontal	$VPP_{yR}\,(cm)$	46 ± 33	40 ± 25	33 ± 26	33 ± 28
	$VPP_{zR}\,(cm)$	3.9 ± 3	5.3 ± 2.6^{a}	5.2 ± 2.1^{a}	6 ± 2.7^{a}
	$VPP_{yL}\,(cm)$	42 ± 29	38 ± 25	34 ± 35	$22 \pm 17^{a,b}$
	$VPP_{zL}\,(cm)$	-3.6 ± 2.3	-6 ± 2.3^{a}	-6.5 ± 2.7^{a}	-6.2 ± 1.8^{a}
	linear fit ($y_R = az_R + b$)	$8.93z + 10$	$8.05z - 2$	$9.6z - 16$	$7.4z - 0.1$
	linear fit ($y_L = az_L + b$)	$-11.5z - 10$	$-8.8z - 9$	$-8.1z - 19$	$-6.65z - 18$
	$R_R^2\,(\%)$	75.3 ± 30	81 ± 24.7	89 ± 16	86 ± 22
	$R_R^2\,(\%)$	83 ± 20	89 ± 10	91 ± 12	94.5 ± 5.6
	$R_L^2\,(\%)$	87 ± 19	82.5 ± 23	77 ± 31	66.5 ± 37.5
	$R_L^2\,(\%)$	91 ± 13.5	87 ± 20	89 ± 10	80 ± 21

Table 2. 3D model parameter

Name	Symbol	Units	Literature	Chosen	Reference
mass	m	kg	60-80	80	(Sharbafi et al., 2013; Budday et al., 2012)
leg stiffness	k	kNm^{-1}	16-26	18	(Sharbafi et al., 2013; McMahon and Cheng, 1990)
leg damping	c	Nsm^{-1}	$400-1200$	900	(Drama and Badri-Spröwitz, 2019)
leg length	l_0	m	$16-26$	1	(Sharbafi et al., 2013)
angle of attack (sag.)	α	$(^\circ)$	$71-78$	$VBLA$	(Sharbafi and Seyfarth, 2016; Abraham et al., 2015)
angle of attack (fron.)	β	$(^\circ)$	$f(\dot{z})$	$VBLA$	(Budday et al., 2012; Sharbafi and Seyfarth, 2016)
dist. Hip-CoM	d	m	0.1	0.1	(Sharbafi et al., 2013; Sharbafi and Seyfarth, 2015)
trunk inertia (sag.)	J_s	kgm^2	4.8	4.8	(Sharbafi and Seyfarth, 2015)
trunk inertia (front.)	J_f	kgm^2	$\approx J_s$	4.8	(Damavandi et al., 2010)
trunk inertia (horiz.)	J_h	kgm^2	$\approx 0.2 J_s$	1	(Damavandi et al., 2010)
gravitational acceleration	g	ms^{-2}	9.81	9.81	

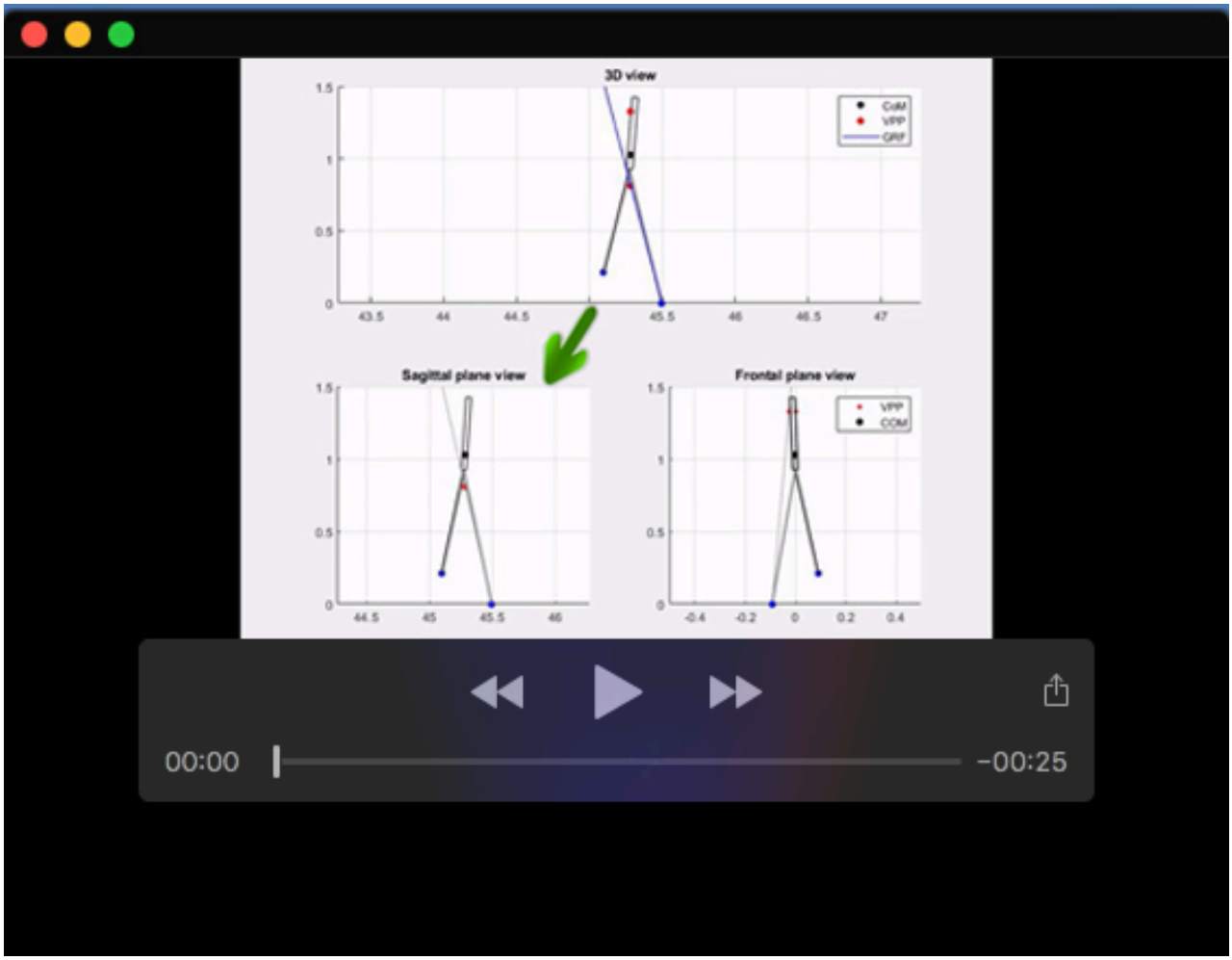

Movie 1. A video of running performance with the proposed 3D model.